Journal of Materials Chemistry B

PAPER

View Article Online
View Journal | View Issue



Cite this: J. Mater. Chem. B, 2019, 7, 3569

# Lysosome-specific sensing and imaging of pH variations *in vitro* and *in vivo* utilizing a near-infrared boron complex†

Yuxiang Shi,[a] Xiangchun Meng,[a] Huiran Yang,[a] Linna Song,[a] Shujuan Liu,*[a] Aqiang Xu,[a] Zejing Chen,[a] Wei Huang *[ab] and Qiang Zhao *[a]

Received 26th December 2018,
Accepted 19th April 2019

DOI: 10.1039/c8tb03353f

rsc.li/materials-b

As a focus issue, the study of lysosomal pH has attracted much attention as it is closely associated with the state of lysosome, which plays a vital role in endocytosis and autophagy. In order to investigate the lysosomal pH, fluorescence bioimaging is one of the most widely-explored approaches. Unfortunately, the probes are insufficient to absorb or emit in the near-infrared (NIR) region, which could minimize photodamage to organisms and maximize tissue penetration in living systems. As a novel family of NIR dyes, hemicyanine has been selected for NIR bioimaging and biosensing owing to its excellent optical properties, easy preparation and good biocompatibility. Employing a classic rhodamine–hemicyanine hybrid, we first designed and synthesized a NIR boron complex (**HCy-BIZ-BF$_2$**) with lysosome-targeting and pH-sensing properties. It is worth mentioning that after **HCy-BIZ** was coordinated with boron fluoride, **HCy-BIZ-BF$_2$** exhibited an improved photostability as well as an enlarged Stokes shift, and was subsequently applied to monitor the lysosomal pH in cells stimulated with chloroquine. Further investigation of pH changes in mice illustrated that **HCy-BIZ-BF$_2$** performed well in detecting the pH in living organisms. Therefore, this concept of boron complex derived from hemicyanine is not only applicable in pH detection, but also conducive for preparing promising novel NIR bioprobes and obtaining precise measurements of physiological parameters in specific physiological processes.



## Introduction

Among various biomarkers, pH is one of the vital parameters closely concerned with cellular components and pathological processes.[1–4] In mammalian cells, organelles work in different pH environments ranging from 4.5 to 8.0.[5,6] Lysosomes, filled with numerous hydrolytic enzymes for cellular hydrolysis,[7,8] exhibit an acidic environment (pH = 4.5–5.5)[9,10] and play a vital role in endocytosis, autophagy and oxidative stress.[11,12] However, an abnormal pH in lysosomes would disrupt the intracellular pH homeostasis and cause many kinds of diseases, including cancers, Alzheimer's disease and cardiopulmonary problems.[13–16] Therefore, it is critical to monitor pH changes in lysosomes and living systems to study cellular functions, which is beneficial to the understanding of these pathological processes.

Fluorescence imaging[17] based on chemical probes has been an important approach for monitoring intracellular pH in the last few decades, especially for its real-time,[18–21] high spatial and temporal resolution imaging.[22–28] Importantly, probes with near-infrared (NIR) absorption and emission are favourable in bioimaging, since they minimize photo damages to organisms[29–32] and maximize tissue penetration to reduce the background interference in the living system.[33–35] However, it is challenging to develop this kind of probe due to the widespread problems of low quantum efficiency, poor photostability as well as small Stokes shift.[36,37] To develop excellent NIR probes, various fluorescence molecules such as cyanine,[38] rhodamine[39–41] and boron dipyrromethene[42,43] have been extensively investigated. Among these probes, hemicyanine, derived from the cyanine family, is known for its desirable optical properties including high fluorescence quantum yield and good biocompatibility.[44–46] Specifically, the rhodamine–hemicyanine hybrid is one of the most effective tools to design new hemicyanine probes.[47,48] Based on a classical hybrid hemicyanine skeleton, numerous strategies have been developed to further improve the photostability and modulate the spectral range,

[a] Key Laboratory for Organic Electronics and Information Displays & Jiangsu Key Laboratory for Biosensors, Institute of Advanced Materials (IAM), Nanjing University of Posts and Telecommunications (NUPT), Nanjing 210023, P. R. China. E-mail: iamqzhao@njupt.edu.cn, provost@nwpu.edu.cn; Fax: +86 25-85866396
[b] Shaanxi Institute of Flexible Electronics (SIFE), Northwestern Polytechnical University (NPU), Xi'an 710072, Shaanxi, China

† Electronic supplementary information (ESI) available. See DOI: 10.1039/c8tb03353f

like commonly-used extensions and hetero-substitutions.[49] Besides, coordination modification through facile chelation between organic molecules and positive ions is a more convenient and effective method.[50–56] Unfortunately, the biosensing platform composed of the rhodamine–hemicyanine hybrid derivatives and positive ions as the coordination center has not yet been established in the subcellular level, especially in the lysosome.

Herein, we designed and synthesized a novel boron complex **HCy-BIZ-BF$_2$** with NIR emission, selective pH-responsiveness and high lysosome-targeting ability to monitor pH variations in the lysosome. In particular, after **HCy-BIZ** was coordinated with boron fluoride, **HCy-BIZ-BF$_2$** exhibited an enlarged Stokes shift (55 nm) and a high photostability, achieving the real-time monitoring of lysosomal pH in HeLa cells stimulated with chloroquine *via* confocal laser scanning microscopy (CLSM). Meanwhile, pH changes in living mice were further investigated using this NIR probe with a high signal-to-noise ratio. It is expected that this strategy of combining a hemicyanine skeleton with boron fluoride could bring more opportunities to NIR fluorescent probes.

## Results and discussion

### Design strategies and optical properties of HCy-BIZ-BF$_2$

To begin with, a novel hemicyanine derivative, **HCy-BIZ**, was prepared by introducing the benzimidazole moiety into the classical hemicyanine skeleton. Its π-conjugate system was subsequently extended, resulting in an obvious red shift (20 nm) in the emission spectrum compared with that of its original structure.[36] As shown in Fig. 1a, **HCy-BIZ** exhibited a NIR absorption and emission, with maximum peaks at 700 and 728 nm, respectively. However, **HCy-BIZ** had a small Stokes shift (28 nm), which could cause an inevitable interference from the excitation source in the fluorescence-collection process.

Then, we resorted to a facile coordination approach through the chelation between **HCy-BIZ** and boron fluoride to form a novel boron complex (**HCy-BIZ-BF$_2$**). This boron coordination led to a rigid hexatomic ring; thus, the intramolecular rotations and vibrations were restricted, contributing to higher stability. The basic synthetic routes are shown in Scheme S1 (ESI†), and the characterizations of all the compounds mentioned are also summarized in the ESI.†

Next, we evaluated the photophysical properties of **HCy-BIZ-BF$_2$**. After **HCy-BIZ** was coordinated with $BF_2$, **HCy-BIZ-BF$_2$** had a maximum absorption at 680 nm and a maximum fluorescence emission at 730 nm, with the Stokes shift increasing from 28 to 55 nm (Fig. 1b). Then, the photostability was investigated through UV-Vis absorption spectra. As exhibited in Fig. 1c, the absorption intensities of **HCy-BIZ-BF$_2$** changed slightly under 30 minute continuous irradiation (660 nm, 250 mW cm$^{-2}$), while those of **HCy-BIZ** decreased obviously, demonstrating that **HCy-BIZ-BF$_2$** has a better photostability than **HCy-BIZ**. These results indicated that the NIR probe **HCy-BIZ-BF$_2$** exhibited outstanding photophysical properties, especially the enlarged Stokes shift and high photostability.

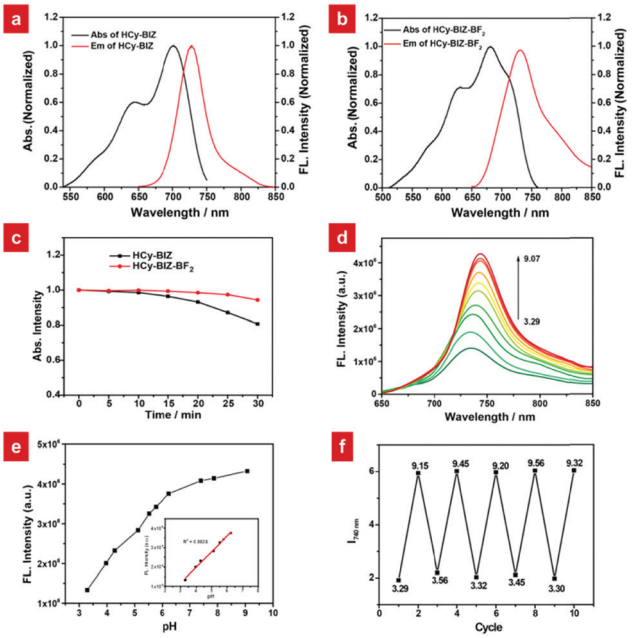


Fig. 1 Optical characteristics of **HCy-BIZ-BF$_2$**. (a) Normalized absorption and emission spectra of **HCy-BIZ** in methyl alcohol (10 μM). (b) Normalized absorption and emission spectra of **HCy-BIZ-BF$_2$** (10 μM) in methyl alcohol. (c) Photostability experiment of **HCy-BIZ-BF$_2$** (10 μM) and **HCy-BIZ** (10 μM) under continuous irradiation (660 nm, 250 mW cm$^{-2}$) in PBS buffer (1% DMSO). (d) Emission spectra of **HCy-BIZ-BF$_2$** (10 μM) in PBS buffer (1% DMSO, $\lambda_{ex}$ = 635 nm) with various pH values (pH = 3.29, 3.97, 4.28, 5.12, 5.52, 5.77, 6.24, 7.40, 7.87, 9.07). (e) The plot of fluorescence intensity (740 nm) over the pH range (3.29–9.07) and the curve (inset) of the emission intensity *versus* the pH range (3.29–6.24). (f) Reversibility experiment of **HCy-BIZ-BF$_2$** (10 μM) in PBS buffer (1% DMSO, $\lambda_{ex}$ = 635 nm).

### pH-responsive properties of HCy-BIZ-BF$_2$

The pH-responsive properties of **HCy-BIZ-BF$_2$** were further studied in PBS with various pH values. As demonstrated in Fig. 1d and Fig. S1a (ESI†), **HCy-BIZ-BF$_2$** was pH-sensitive in both emission and absorption spectra. The emission intensity of **HCy-BIZ-BF$_2$** displayed an obvious increase in acidic (pH = 3.29 to 6.24) conditions, while it changed slightly in alkaline (pH = 7.40 to 9.07) media (Fig. 1d). In the meantime, a smaller red shift and a slight increase in absorption were observed, accompanied by the colour of the solution changing from blue (pH = 3.29) to green (pH = 9.07) (Fig. S1b, ESI†). This trend was in line with the calculated absorption spectra of **HCy-BIZ-BF$_2$** (Fig. S2b, ESI†). Besides, the good linear relationship of the fluorescence intensity *versus* pH values exhibited a high sensitivity of **HCy-BIZ-BF$_2$** towards pH changes, especially in the range of 3.29 to 6.24 (Fig. 1e). According to the Henderson–Hasselbalch equation (Fig. S4, ESI†), the corresponding p$K_a$ was calculated to be 5.03, illustrating that **HCy-BIZ-BF$_2$** could sense slight pH variations in the range of 4.4–6.2, which covers the lysosomal pH values in both normal and abnormal situations.

According to the above-mentioned pH-responsive phenomena, the responsive mechanism of **HCy-BIZ-BF$_2$** towards $H^+$ was investigated by the $^1$H NMR titration experiment, which was conducted

 

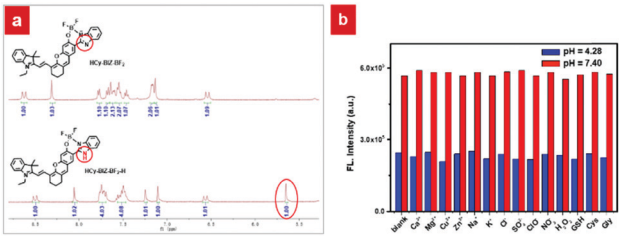


Fig. 2 (a) $^1$H NMR spectra of **HCy-BIZ-BF$_2$** in DMSO-$d_6$ without or with TFA. (b) Emission spectra of **HCy-BIZ-BF$_2$** (10 μM) with different ions, ROS and bioactive molecules. $\lambda_{ex}$ = 635 nm, $\lambda_{em}$ = 740 nm.

by adding trifluoroacetic acid (TFA) dropwise into the **HCy-BIZ-BF$_2$** solution (DMSO-$d_6$). As shown in Fig. 2a, upon the reaction of **HCy-BIZ-BF$_2$** with TFA, the proton peaks at the low field (7.2–7.5 ppm) gradually merged together, while the characteristic peak corresponding to the NH of **HCy-BIZ-BF$_2$-H** appeared at $d$ = 5.65 ppm, confirming the protonation process and the existence of a H atom. Thus, the pH-responsive mechanism is illustrated in Scheme 1. To be specific, fluctuations in the $H^+$ concentration could influence the protonation/deprotonation processes of the imine group, resulting in the changes in fluorescence signals.

Subsequently, the selectivity experiments were conducted in the presence of various biological species. As depicted in Fig. 2b and Fig. S3 (ESI†), the presence of diverse ions ($Ca^{2+}$, $Mg^{2+}$, $Cu^{2+}$, $H_2O_2$, *etc.*) and biologically relevant species, such as L-glutathione (GSH), glycine (Gly) and cysteine (Cys), did not cause any observable fluorescence intensity changes. Importantly, **HCy-BIZ-BF$_2$** also exhibited excellent reversibility between pH 3.5 and 9.2 (Fig. 1f), which was beneficial to the precise and reversible measurements of pH values. Generally speaking, **HCy-BIZ-BF$_2$** showed great potentiality for NIR pH detection in complicated intracellular environments, especially in acidic media.

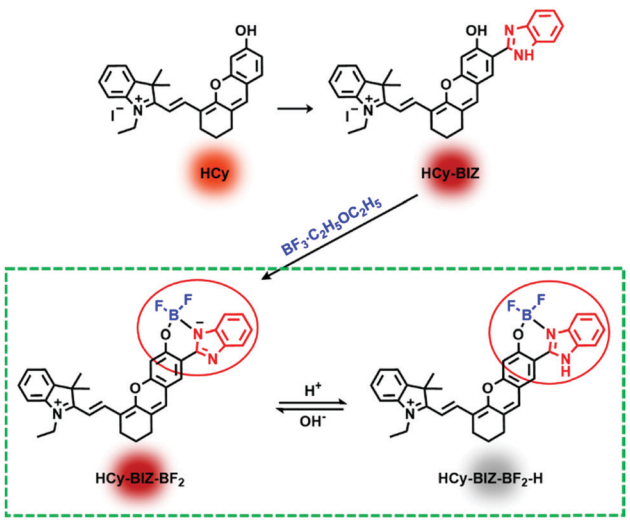


Scheme 1 Design concept and responsive mechanism of **HCy-BIZ-BF$_2$** towards $H^+$.

## Evaluations of HCy-BIZ-BF$_2$ in living cells

Before the *in vivo* and *in vitro* experiments, the cytotoxicity of **HCy-BIZ-BF$_2$** towards HeLa cells was evaluated using the 3-(4,5-dimethyl-2-thiazolyl)-2,5-diphenyltetrazolium bromide (MTT) assay. After 24 hour incubation, HeLa cells retained around 90% viability at various incubating concentrations of **HCy-BIZ-BF$_2$** from 0 to 50 μM, indicating that **HCy-BIZ-BF$_2$** is biocompatible in living cells (Fig. S3, ESI†). The merits of the probe's NIR emission are depicted in Fig. 3. While observing cells without any fluorescent probe, nearly no autofluorescence signals were obtained under the irradiation at 635 nm, while evident background fluorescence could be observed when excited by the 405 nm laser (Fig. 3a). These differences were further analysed by the statistical data collected from the regions of interests (ROIs) in the cell imaging results, where the mean value ($I_{cell}/I_{blank}$) of the NIR signals upon excitation at 635 nm was only a half of that under the irradiation at 405 nm (Fig. 3b).

These data showed that the NIR-emission probe **HCy-BIZ-BF$_2$** showed a superb anti-interference performance, which could effectively reduce the interferences from the background.

Photostability is another important property, especially for small-molecule fluorescence probes. To compare the photostability of **HCy-BIZ-BF$_2$** and DND-99 (an available lysosome tracker),

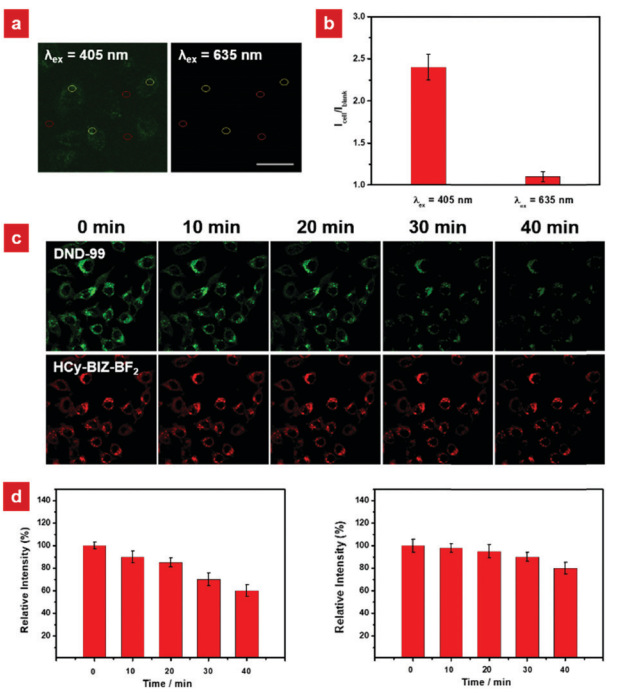


Fig. 3 (a) Autofluorescence experiments of HeLa cells under different detection conditions ($\lambda_{ex}$ = 405 nm, $\lambda_{em}$ = 450–550 nm and $\lambda_{ex}$ = 635 nm, $\lambda_{em}$ = 650–750 nm). (b) The pixel intensity ratios ($I_{cell}/I_{blank}$) from the cell regions (yellow circles) and non-cell regions (red circles) were applied to evaluate the relative autofluorescence in these ROIs. (c) Fluorescence images ($\lambda_{em}$ = 540–600 nm) of cells treated with DND-99 under different time domains and **HCy-BIZ-BF$_2$** ($\lambda_{em}$ = 650–750 nm) under different time domains. (d) The histograms of the relative emission intensity of DND-99 (left) and **HCy-BIZ-BF$_2$** (right) in cells under different time domains. These data were exhibited as the mean ± SD. Scale bar: 30 μm.

the related experiment in HeLa cells was conducted. The cells were simultaneously excited by the continuous lasers (532 nm and 660 nm), and the fluorescence images were collected through different channels (green channel, 540–600 nm and red channel, 670–750 nm). As exhibited in Fig. 3c, the fluorescence intensity of the green channel (DND-99) was bleached quickly over time with a greater decline to around 60% of the initial intensity after 40 min. On the contrary, a small emission decrease (less than 10%, Fig. 3d) of **HCy-BIZ-BF$_2$** was observed after 40-minute irradiation, verifying good photostability in living cells. These results illustrated that **HCy-BIZ-BF$_2$** has an excellent anti-interference property and high intracellular photostability, which reveal the promising application of **HCy-BIZ-BF$_2$** in pH-related bioimaging.

### Detection of lysosomal pH variations in living cells

Based on the excellent NIR emission, good biocompatibility, high anti-interference property and photostability, the probe **HCy-BIZ-BF$_2$** was applied to evaluate its distribution in living cells. After the incubation of HeLa cells with **HCy-BIZ-BF$_2$** for 15 min, the cell cytoplasm exhibited an obvious NIR fluorescence (Fig. 4a). As shown in the Z-scan imaging results, **HCy-BIZ-BF$_2$** was distributed extensively from top to bottom, which can be demonstrated in detail by the enlarged images of the cells' cross section (*X*–*Z*) and longitudinal section (*Y*–*Z*), verifying that **HCy-BIZ-BF$_2$** can quickly enter and sufficiently permeate cells. Interestingly, by performing the co-stained experiment with a commercial lysosome tracker (DND-99), it was found that **HCy-BIZ-BF$_2$** tended to accumulate in lysosomes. As depicted in Fig. 4c, the fluorescence images of **HCy-BIZ-BF$_2$** merged rather well with that of DND-99, with a high Pearson's Correlation Coefficient (0.92). In addition, the emission intensity profiles of the ROIs across the cells were selected to study the overlap images, and a relatively high overlap was found in Fig. 4d. To further demonstrate this lysosomal specificity, mitochondrion-related experiments were also conducted by the co-incubation of HeLa cells with **HCy-BIZ-BF$_2$** and Mito-Tracker Green. In contrast, the cell images of **HCy-BIZ-BF$_2$** and Mito-Tracker Green displayed a totally different distribution with a lower Pearson's Correlation coefficient (0.56), as well as the distinct emission intensity plot of the ROIs (Fig. 4d). Besides, the experimental results of **HCy-BIZ-BF$_2$** co-stained with commercial trackers of the endoplasmic reticulum and Golgi apparatus also exhibited low Pearson's correlation coefficients (Fig. S6, ESI†). Therefore, these results prove that the NIR probe **HCy-BIZ-BF$_2$** is an excellent lysosome-targeting probe with high selectivity.

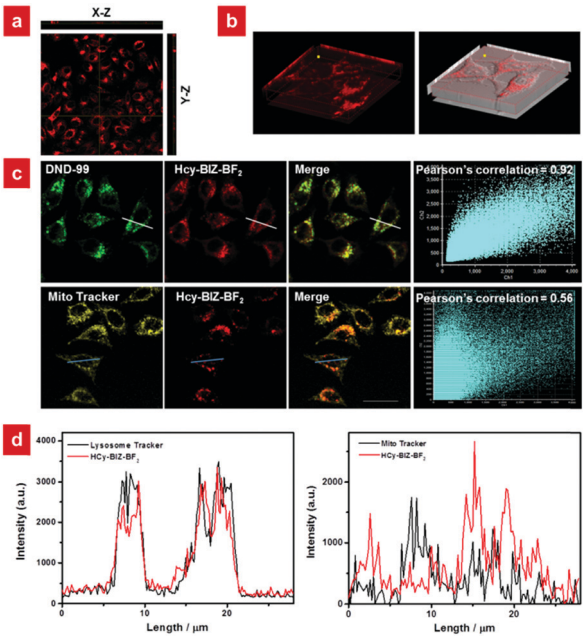


Fig. 4 (a) CLSM images of HeLa cells incubated with **HCy-BIZ-BF$_2$** (100 nM) through Z-scan mode. (b) Enlarged views of the fluorescence image and DIC ($\lambda_{ex}$ = 635 nm, $\lambda_{em}$ = 650–750 nm). (c) Colocalization images of HeLa cells incubated with **HCy-BIZ-BF$_2$** (50 nM, $\lambda_{ex}$ = 635 nm, $\lambda_{em}$ = 650–750 nm) and DND-99 (50 nM, $\lambda_{ex}$ = 515 nm, $\lambda_{em}$ = 540–600 nm), along with the fluorescence intensity correlation plot of **HCy-BIZ-BF$_2$** and DND-99. Colocalization images of HeLa cells incubated with **HCy-BIZ-BF$_2$** (50 nM, $\lambda_{ex}$ = 635 nm, $\lambda_{em}$ = 650–750 nm) and Mito-Tracker Green (200 nM, $\lambda_{ex}$ = 488 nm, $\lambda_{em}$ = 500–560 nm) along with their fluorescence intensity correlation plot. (d) Intensity profiles within the ROI 1 (DND-99 experiment) and ROI 2 (Mito-Tracker Green experiment) across HeLa cells. Scale bar: 30 μm.

Subsequently, **HCy-BIZ-BF$_2$** was used to evaluate the variations of pH values in living cells. The experiment was conducted using a high $K^+$ buffer and nigericin in bath solutions of various pH (4.14, 4.97, 6.23, 7.16, 8.34). As shown in Fig. 5a, the fluorescence intensity of **HCy-BIZ-BF$_2$** increased proportionally with the pH varying from 4.14 to 8.34. Accordingly, the intracellular pH standard curve was obtained (Fig. 5b) with the regression equation $Y = 0.2685x - 1.116$ ($R^2 = 0.98853$).

Then, **HCy-BIZ-BF$_2$** was applied to monitor the pH fluctuations in the lysosome. It is reported that the lysosome is at the terminal of the endocytosis pathway, and it has a highly acidic lumen with pH values ranging from 4.5 to 5.5.[57] Its pH values, however, can grow gradually under the stimulation of chloroquine (a kind of antimalarial drug). Under the same conditions ($\lambda_{ex}$ = 635 nm, $\lambda_{em}$ = 650–750 nm), the related fluorescence

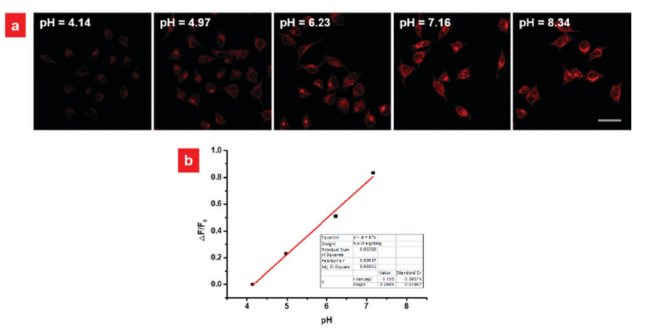


Fig. 5 (a) CLSM images of HeLa cells incubated with **HCy-BIZ-BF$_2$** (100 nM, $\lambda_{ex}$ = 635 nm, $\lambda_{em}$ = 650–750 nm) in different pH buffer solutions. (b) Intracellular pH calibration curve of **HCy-BIZ-BF$_2$** in HeLa cells from (a) $\Delta F/F_0$ (*F*: stands for fluorescence intensity at different pH values; $F_0$: means fluorescence intensity at pH = 4.14). Scale bar: 40 μm.

 

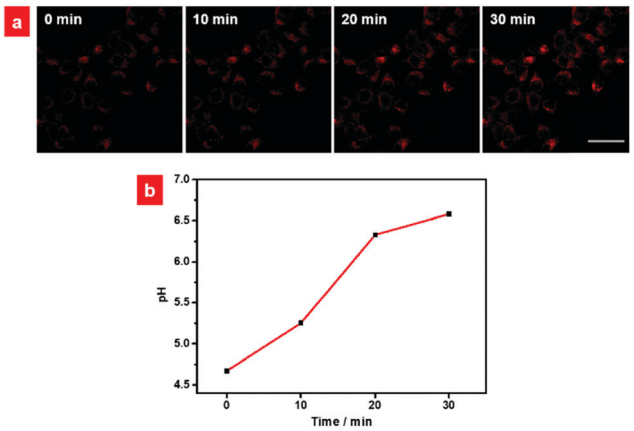


Fig. 6 Time courses of pH responses in lysosomes caused by chloroquine. (a) HeLa cells were incubated with **HCy-BIZ-BF$_2$** (100 nM) for 15 min, and then treated with chloroquine (100 μM). The fluorescence images were recorded at different times. (b) The plot of time-dependent pH values. Scale bar: 30 μm.

images of HeLa cells stimulated by chloroquine were captured (Fig. 6a). According to the pH standard curve, the determination of the time-dependent changes of the pH values was plotted (Fig. 6b). Specifically, the initial pH value in the lysosomes under normal incubation was calculated to be 4.67. After the cells were stimulated with chloroquine for 10 min, the pH increased to 5.25 with enhanced fluorescence intensity, and finally increased to 6.58 after 30 minute stimulation. These results demonstrated that **HCy-BIZ-BF$_2$** is an efficient NIR probe that can monitor the lysosomal pH variations in cells treated with chloroquine in real time.

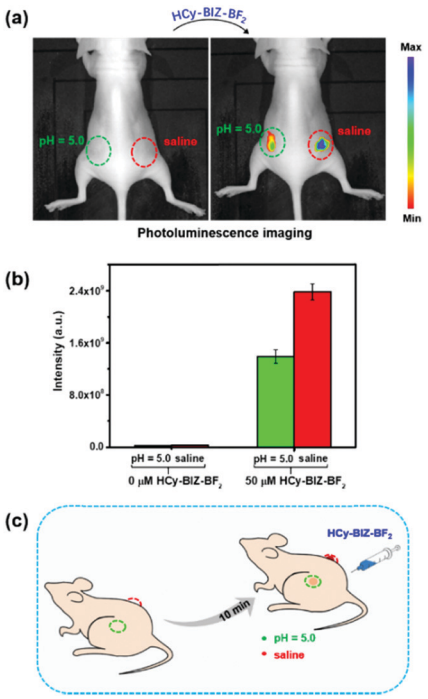


Fig. 7 (a) Photoluminescence images of a mouse labeled with **HCy-BIZ-BF$_2$**. Saline (60 μL, pH 6.9) and PBS solution (60 μL, pH = 5.0) were injected into two adjacent spots on the back of the nude mouse. Then, **HCy-BIZ-BF$_2$** (60 μL, 50 μM) was subcutaneously injected into these two different locations ($\lambda_{ex}$ = 640 nm, $\lambda_{em}$ = 710 ± 40 nm). (b) The photoluminescence intensity of parts injected with saline (red circle) and pH solution (green circle) (c) A sketch of photoluminescence imaging in the labeled living mouse.

### Mapping of pH changes in a living mouse model

The excellent photophysical properties and the robust pH-sensitive response in cells provided the basis that **HCy-BIZ-BF$_2$** can be used for pH detection in living mice. First, saline (60 μL, pH = 6.9) and PBS (60 μL, pH = 5.0) were injected subcutaneously into two sides on the back of a nude mouse. Under the excitation at 640 nm, the NIR emission signals of **HCy-BIZ-BF$_2$** in the mouse could be monitored by the *in vivo* imaging system. As depicted in Fig. 7a, without **HCy-BIZ-BF$_2$**, there was no observable photoluminescence in the right back (saline, pH = 6.9) and the left back (PBS, pH = 5.0) of the mouse. After the mouse was treated for 5 min, the same volume of **HCy-BIZ-BF$_2$** solution (60 μL, 50 μM) was subcutaneously injected into the two different pH areas. After 10 minute incubation, the emission intensity of the right back was much stronger than that of the left back (Fig. 7b). The statistical data further explained this trend that the fluorescence intensity of **HCy-BIZ-BF$_2$** in the saline spot was about 1.3 times that in the acidic site. According to the above-described experiments, this evident fluorescence signal enhancements could be caused by the deprotonation of **HCy-BIZ-BF$_2$** in the saline location. In short, **HCy-BIZ-BF$_2$** is characterised with superb properties as a NIR fluorescence probe for pH detection in living systems.

## Conclusions

In summary, we first introduced a novel strategy of a boron complex on the basis of a classical rhodamine–hemicyanine hybrid, and designed a novel pH-sensing lysosomal probe, **HCy-BIZ-BF$_2$**. Meanwhile, we compared the primary properties and biological applications of **HCy-BIZ-BF$_2$** with those of the recently reported lysosomal probes in Table S1 (ESI†). It is concluded that **HCy-BIZ-BF$_2$** was characterized with NIR emission, linear pH responsiveness and lysosome targetability. Most importantly, after the chelation with boron fluoride, **HCy-BIZ-BF$_2$** possesses an enlarged Stokes shift and improved photostability, which is superior to its precursor. Subsequently, **HCy-BIZ-BF$_2$** was applied to monitor the pH in lysosomes stimulated with chloroquine, and further to successfully investigate the changes of pH in living mice with a high signal-to-noise ratio. It is accordingly believed that this concept of boron complex combined with tunable classic hemicyanine would offer more chances to construct novel NIR fluorescent probes.

## Experimental section

The detailed information of instruments, materials, synthesis and characterization of all compounds, cell cultivation, *in vitro*/*in vivo* imaging were provided in the ESI.†

### Animal models

All the nude mice were purchased from the Comparative Medicine Centre of Yangzhou University. All the animal-based experiments were performed in compliance with the criteria of the National Regulation of China for Care and Use of Laboratory Animals and approved by the Jiangsu Administration of Experimental Animals.

## Conflicts of interest

There are no conflicts to declare.

## Acknowledgements

This work was supported by the National Funds for Distinguished Young Scientists (61825503), National Natural Science Foundation of China (51473078 and 21671108), National Program for Support of Top-Notch Young Professionals, Scientific and Technological Innovation Teams of Colleges and Universities in Jiangsu Province (TJ215006), Priority Academic Program Development of Jiangsu Higher Education Institutions (YX03001), China Postdoctoral Science Foundation funded project (2016M601789), and Jiangsu Province Postdoctoral Science Foundation funded project (1701034A).

## Notes and references

1 J. R. Casey, S. Grinstein and J. Orlowski, *Nat. Rev. Mol. Cell Biol.*, 2010, **11**, 50–61.
2 J. P. Luzio, P. R. Pryor and N. A. Bright, *Nat. Rev. Mol. Cell Biol.*, 2007, **8**, 622–632.
3 B. Tang, F. Yu, P. Li, L. Tong, X. Duan, T. Xie and X. Wang, *J. Am. Chem. Soc.*, 2009, **131**, 3016–3023.
4 S. Wu, Z. Li, J. Han and S. Han, *Chem. Commun.*, 2011, **47**, 11276–11278.
5 J. Y. Han and K. Burgess, *Chem. Rev.*, 2010, **110**, 2709–2728.
6 J. T. Hou, W. X. Ren, K. Li, J. Seo, A. Sharma, X. Q. Yu and J. S. Kim, *Chem. Soc. Rev.*, 2017, **46**, 2076–2090.
7 P. Saftig and J. Klumperman, *Nat. Rev. Mol. Cell Biol.*, 2009, **10**, 623–635.
8 S. J. Lee, K. S. Cho and J. Y. Koh, *Glia*, 2009, **57**, 1351–1361.
9 Y. Yue, F. Huo, S. Lee, C. Yin and J. Yoon, *Analyst*, 2016, **142**, 30–41.
10 S. Chen, Y. Hong, Y. Liu, J. Liu, C. W. T. Leung, M. Li, R. T. K. Kwok, E. Zhao, J. W. Y. Lam, Y. Yu and B. Z. Tang, *J. Am. Chem. Soc.*, 2014, **136**, 11196.
11 C. Watts, *Biochim. Biophys. Acta*, 2012, **1824**, 14–21.
12 K. A. Christensen, J. T. Myers and J. A. Swanson, *J. Cell Sci.*, 2002, **115**, 599–607.
13 D. Ellis and R. C. Thomas, *Nature*, 1976, **262**, 224–225.
14 R. Zhang, S. G. Kelsen and J. C. Lamanna, *J. Appl. Physiol.*, 1990, **68**, 1101–1106.
15 H. Izumi, T. Torigoe, H. Ishiguchi, H. Uramoto, Y. Yoshida, M. Tanabe, T. Ise, T. Murakami, T. Yoshida, M. Nomoto and K. Kohno, *Cancer Treat. Rev.*, 2003, **29**, 541–549.
16 H. Zhu, J. L. Fan, Q. L. Xu, H. L. Li, J. Y. Wang, P. Gao and X. J. Peng, *Chem. Commun.*, 2012, **48**, 11766–11768.
17 A. Ettinger and T. Wittmann, *Methods Cell Biol.*, 2014, **123**, 77–94.
18 Q. Wan, S. Chen, W. Shi, L. Li and H. Ma, *Angew. Chem., Int. Ed.*, 2014, **53**, 10916–10920.
19 K.-K. Yu, K. Li, J.-T. Hou, H.-H. Qin, Y.-M. Xie, C.-H. Qian and X.-Q. Yu, *RSC Adv.*, 2014, **4**, 33975–33980.
20 K. E. Beatty, J. D. Fisk, B. P. Smart, Y. Y. Lu, J. Szychowski, M. J. Hangauer, J. M. Baskin, C. R. Bertozzi and D. A. Tirrell, *ChemBioChem*, 2010, **11**, 2092–2095.
21 M. Grossi, M. Morgunova, S. Cheung, D. Scholz, E. Conroy, M. Terrile, A. Panarella, J. C. Simpson, W. M. Gallagher and D. F. O'Shea, *Nat. Commun.*, 2016, **7**, 10855.
22 W. Luo, H. Jiang, X. Tang and W. Liu, *J. Mater. Chem. B*, 2017, **5**, 4768–4773.
23 B. Dong, X. Song, C. Wang, X. Kong, Y. Tang and W. Lin, *Anal. Chem.*, 2016, **88**, 4085–4091.
24 J. Liu, Y. Q. Sun, Y. Huo, H. Zhang, L. Wang, P. Zhang, D. Song, Y. Shi and W. Guo, *J. Am. Chem. Soc.*, 2014, **136**, 574–577.
25 A. Becker, C. Hessenius, K. Licha, B. Ebert, U. Sukowski, W. Semmler, B. Wiedenmann and C. Grotzinger, *Nat. Biotechnol.*, 2001, **19**, 327–331.
26 K. Vellaisamy, G. Li, C. N. Ko, H. J. Zhong, S. Fatima, H. Y. Kwan, C. Y. Wong, W. J. Kwong, W. Tan, C. H. Leung and D. L. Ma, *Chem. Sci.*, 2018, **9**, 1119–1125.
27 Z. Dong, Q. Han, Z. Mou, G. Li and W. Liu, *J. Mater. Chem. B*, 2018, **6**, 1322–1327.
28 S. Xia, J. Wang, J. Bi, X. Wang, M. Fang, T. Phillips, A. May, N. Conner, M. Tanasova, F. T. Luo and H. Liu, *Sens. Actuators, B*, 2018, **265**, 699–708.
29 S. O. McDonnell and D. F. O'Shea, *Org. Lett.*, 2006, **8**, 3493–3496.
30 L. Fan, Y. J. Fu, Q. L. Liu, D. T. Lu, C. Dong and S. M. Shuang, *Chem. Commun.*, 2012, **48**, 11202–11204.
31 D. Aigner, S. M. Borisov, P. Petritsch and I. Klimant, *Chem. Commun.*, 2013, **49**, 2139–2141.
32 H. Lee, W. Akers, K. Bhushan, S. Bloch, G. Sudlow, R. Tang and S. Achilefu, *Bioconjugate Chem.*, 2011, **22**, 777–784.
33 J. Madsen, I. Canton, N. J. Warren, E. Themistou, A. Blanazs, B. Ustbas, X. Tian, R. Pearson, G. Battaglia, A. L. Lewis and S. P. Armes, *J. Am. Chem. Soc.*, 2013, **135**, 14863–14870.
34 P. Li, X. Duan, Z. Z. Chen, Y. Liu, T. Xie, L. B. Fang, X. R. Li, M. Yin and B. Tang, *Chem. Commun.*, 2011, **47**, 7755–7757.
35 F. Yu, P. Li, P. Song, B. Wang, J. Zhao and K. Han, *Chem. Commun.*, 2012, **48**, 4980–4982.
36 W. Qin, T. Rohand, M. Baruah, A. Stefan, M. V. der Auweraer, W. Dehaen and N. Boens, *Chem. Phys. Lett.*, 2006, **420**, 562–568.
37 U. Balijapalli and S. K. Iyer, *Eur. J. Org. Chem.*, 2015, 5089–5098.
38 W. Sun, S. Guo, C. Hu, J. Fan and X. Peng, *Chem. Rev.*, 2016, **116**, 7768–7817.
39 M. Beija, C. A. Afonso and J. M. Martinho, *Chem. Soc. Rev.*, 2009, **38**, 2410–2433.

 

40 J. Wang, S. Xia, J. Bi, Y. Zhang, M. Fang, R. L. Luck, Y. Zeng, T.-H. Chen, H.-M. Lee and H. Liu, *J. Mater. Chem. B*, 2019, **7**, 198–209.
41 G. K. Vegesna, J. Janjanam, J. Bi, F.-T. Luo, J. Zhang, C. Olds, A. Tiwari and H. Liu, *J. Mater. Chem. B*, 2014, **2**, 4500–4508.
42 S. Kolemen and E. U. Akkaya, *Coord. Chem. Rev.*, 2018, **354**, 121–134.
43 M. Zhu, P. Xing, Y. Zhou, L. Gong, J. Zhang, D. Qi, Y. Bian, H. Du and J. Jiang, *J. Mater. Chem. B*, 2018, **6**, 4422–4426.
44 L. Yuan, W. Lin, S. Zhao, W. Gao, B. Chen, L. He and S. Zhu, *J. Am. Chem. Soc.*, 2012, **134**, 13510–13523.
45 J. Zhang, C. Li, R. Zhang, F. Zhang, W. Liu, X. Liu, S. M. Lee and H. Zhang, *Chem. Commun.*, 2016, **52**, 2679–2682.
46 C. Han, H. Yang, M. Chen, Q. Su, W. Feng and F. Li, *ACS Appl. Mater. Interfaces*, 2015, **7**, 27968–27975.
47 J. Wang, S. Xia, J. Bi, M. Fang, W. Mazi, Y. Zhang, N. Conner, F. T. Luo, H. P. Lu and H. Liu, *Bioconjugate Chem.*, 2018, **29**, 1406–1418.
48 L. Yuan, W. Lin, Y. Yang and H. Chen, *J. Am. Chem. Soc.*, 2012, **134**, 1200–1211.
49 Y. Li, Y. Wang, S. Yang, Y. Zhao, L. Yuan, J. Zheng and R. Yang, *Anal. Chem.*, 2015, **87**, 2495–2503.
50 P. Tao, Y. Miao, H. Wang, B. Xu and Q. Zhao, *Chem. Rec.*, 2018, DOI: 10.1002/tcr.201800139.
51 H. Mtiraoui, R. Gharbi, M. Msaddek, Y. Bretonnière, C. Andraud, P.-Y. Renard and C. Sabot, *RSC Adv.*, 2016, **6**, 86352–86360.
52 W. Duan, Q. Liu, Y. Huo, J. Cui, S. Gong and Z. Liu, *Org. Biomol. Chem.*, 2018, **16**, 4977–4984.
53 H. Xiao, P. Li, W. Zhang and B. Tang, *Chem. Sci.*, 2016, **7**, 1588–1593.
54 D. L. Ma, C. Wu, G. Li and C. H. Leung, *J. Anal. Test.*, 2018, **2**, 77–89.
55 D.-L. Ma, C.-M. Che and S.-C. Yan, *J. Am. Chem. Soc.*, 2009, **131**, 1835–1846.
56 H. Sun, W. Li, Z. Z. Dong, C. Hu, C. H. Leung, D. L. Ma and K. Ren, *Biosens. Bioelectron.*, 2018, **99**, 361–367.
57 C. Settembre, A. Fraldi, D. L. Medina and A. Ballabio, *Nat. Rev. Mol. Cell Biol.*, 2013, **14**, 283–296.